Engineering 29 (2023) 159–167

Contents lists available at ScienceDirect

Engineering

journal homepage: www.elsevier.com/locate/eng

Research
Environmental Engineering—Article

Interactions of Microplastics and Methane Seepage in the Deep-Sea Environment

Jing-Chun Feng [a,b,*], Zhifeng Yang [a,b], Wenliang Zhou [a], Xingwei Feng [b], Fuwen Wei [a], Bo Li [b], Chuanxin Ma [b], Si Zhang [a,*], Linlin Xia [b], Yanpeng Cai [a,b], Yi Wang [c,d]

[a] Southern Marine Science and Engineering Guangdong Laboratory (Guangzhou), Guangzhou 511458, China
[b] Guangdong Provincial Key Laboratory of Water Quality Improvement and Ecological Restoration for Watersheds, Institute of Environmental and Ecological Engineering, Guangdong University of Technology, Guangzhou 510006, China
[c] Key Laboratory of Gas Hydrate, Guangzhou Institute of Energy Conversion, Chinese Academy of Sciences, Guangzhou 510640, China
[d] Guangzhou Center for Gas Hydrate Research, Chinese Academy of Sciences, Guangzhou 510640, China

ARTICLE INFO

Article history:
Received 24 March 2022
Revised 20 June 2022
Accepted 4 August 2022
Available online 17 September 2022

Keywords:
Microplastics
Anaerobic oxidation of methane
Cold seeps
Diversity index
Fragmentation
Gas hydrates

ABSTRACT

Microplastics (MPs) are important exempla of the Anthropocene and are exerting an increasing impact on Earth's carbon cycle. The huge imbalance between the MPs floating on the marine surface and those that are estimated to have been introduced into the ocean necessitates a detailed assessment of marine MP sinks. Here, we demonstrate that cold seep sediments, which are characterized by methane fluid seepage and a chemosynthetic ecosystem, effectively capture and accommodate small-scale (< 100 μm) MPs, with 16 types of MPs being detected. The abundance of MPs in the surface of the sediment is higher in methane-seepage locations than in non-seepage areas. Methane seepage is beneficial to the accumulation, fragmentation, increased diversity, and aging of MPs. In turn, the rough surfaces of MPs contribute to the sequestration of the electron acceptor ferric oxide, which is associated with the anaerobic oxidation of methane (AOM). The efficiency of the AOM determines whether the seeping methane (which has a greenhouse effect 83 times greater than that of CO_2 over a 20-year period) can enter the atmosphere, which is important to the global methane cycle, since the deep-sea environment is regarded as the largest methane reservoir associated with natural gas hydrates.

1. Introduction

Microplastics (MPs) have been attracting increasing attention in the oceanic environment, as more than ten million tonnes of plastic enter the ocean due to anthropological activity every year [1]. MPs are particles of plastic smaller than 5 mm in length. Global estimates indicate a large imbalance between the amount of MPs estimated to have been introduced into the ocean and the amount floating on the ocean surface [2]. The missing MPs (particularly those < 1 mm) in the surface oceans have garnered widespread attention. Several possible reasons for the missing MPs have been proposed, such as ingestion by zooplankton [3], rapid degradation and decomposition through the effects of light and water [4], and transportation to the deeper layer of the ocean [5].

The spread of MPs throughout the unknown and remote deep-sea areas has been verified, and MPs have been detected in the Mediterranean Sea and the Atlantic Ocean at water depths ranging from 1176 to 4844 m [6]. Modeling results have revealed that the deep sea is the largest natural MP sink [7], and MPs have been widely discovered in continental slopes [8], submarine canyons [9], deep-sea trenches [10], and abyssal plains [11]. MPs can be ingested by deep-sea animals; moreover, MPs can carry other pollutants, such as heavy metals, dyes, and persistent pollutants, thereby bringing combined pollution to marine ecosystems [12]. Nevertheless, the mechanism by which MPs sink into the deep sea is unclear, and the amount of MPs that can be buried in the deep-sea floor at a global scale necessitates attention [13].

Oceanic currents, which induce the vertical and horizontal transfer of a large volume of water, are conducive to the transportation of MPs from the surface to the deeper ocean. Offshore convection [14], saline subduction [15], gravity currents, coastal storms, and the deep thermohaline current are also important

* Corresponding authors.
E-mail addresses: fengjc@gdut.edu.cn (J.-C. Feng), zhsimd@scsio.ac.cn (S. Zhang).

https://doi.org/10.1016/j.eng.2022.08.009

oceanic factors [16]. MPs seem to be more likely to accumulate in the deep-sea trenches and canyons [17], as these formations promote the creation of gravity flows that can cause the negatively buoyant MPs to gather in such regions [18]. Other areas that can influence the down-welling of the flow, such as Taylor columns on seamounts, can enhance the retention of MPs as well [19].

However, special regions that can impact water currents and extreme ecosystems have been overlooked. Cold seeps, which are unique deep-sea environments where methane-rich fluids seep from the seafloor into the water zone, sustain the richest chemosynthetic ecosystems [20]. In such environments, methane seepage promotes the bottom current in the deep-sea floor, which is the dominant factor influencing the distribution of particles in the deep-sea environment [16]. Thus, we hypothesize that this methane flow can affect the distribution of MPs in deep-sea sediments. The upwelling methane flow lifts denser and colder particles and entrains them into the fluid flow, and the strong stratification of the water layer influences the energy transport of the plume flow [21]. Once the upwelling flow can no longer raise the denser flow, the plume water substantially descends, creating an intrusion layer [22]. In particular, large-scale recirculation flow can exist adjacent to the seepage point within the strong plume pattern, resulting in a high concentration of methane and particles in the water [23]. MPs can also be enriched and drawn toward the methane-seepage point due to the intrusion flow and recirculation flow.

However, the occurrence of MPs in cold seeps, especially the role of methane flow in MP accumulation, remains unknown. In addition, it is necessary to clarify how to identify fine-scale (< 100 μm) MPs in cold seeps, because small-scale MPs can be more easily ingested by organisms [24] and can potentially cause damage to these special and fragile ecosystems. Due to MPs' rough surfaces, these particles can accommodate abundant infochemicals (e.g., dimethyl sulfide) and microorganisms [25] and can influence the element cycles (e.g., the carbon cycle) of the Earth system [26]. Thus, it is essential to identify the occurrence and distribution characteristics of MPs in cold seeps and the effectiveness of their sequestration after they enter seafloor sediments.

In this study, we experimentally investigated the full-size range (0–5000 μm) of MPs in cold seep sediments with different methane-seepage characteristics (Fig. 1 [16,19,27–30]). The Haima cold seep in the northern part of the South China Sea was chosen as the study area, as it is a typical continental cold seep [31]. The geological and ecological features of the study area are shown in Figs. S1 and S2 in Appendix A, respectively. To overcome the difficulty of identifying MPs smaller than 63 μm via the traditional Fourier-transform infrared spectroscopy (FTIR) method [16], we used a laser direct infrared (LDIR) chemical imaging system to detect small-scale MPs. We observed that the cold seep is a major sink of MPs, especially small MPs (< 100 μm). The effects of methane seepage on the occurrence, abundance, fragmentation, diversity, and aging of MPs were investigated. Moreover, iron (Fe) enrichment on the MPs was found to promote the anaerobic oxidation of methane (AOM), which is an important filter that impedes the entrance of large quantities of methane into the atmosphere [32].

2. Materials and methods

2.1. Sediment core samples and chemicals

Four sediment core samples were collected from the Haima cold seep area in September 2020. Sub-sediment samples were obtained for MP extraction by cutting the core into small pieces; the samples originated from the 0–10 cm depth interval. All of the chemicals used in this study, including H_2O_2, $ZnCl_2$, HCl, and $(NaPO_3)_6$, were reagent grade or higher and were supplied by Sinopharm (China). The ultrapure water (18.2 $m\Omega \cdot cm^{-1}$) used in this study was prepared using a Millipore water system (ELGA Purelab Chorus PC1LSCXM2, UK).

2.2. Pretreatment of sediment core samples

The four sediment samples were transferred to metal trays for pre-rinsing, and were then placed in clean paper bags for freeze-drying at –80 °C to remove all moisture. After drying, 50 g of each sample was weighed and ground using a precleaned mortar and pestle. The ground sample was then poured into a 2 L glass beaker. Next, 200 mL of 30% H_2O_2 solution was slowly added to the beaker to dissolve the sample. The beaker was covered with aluminum foil and incubated at 60 °C in a water bath for 3–5 days until the visible suspended matter disappeared.

2.3. MP extraction, identification, and analysis

The H_2O_2 solution containing the MPs was repeatedly extracted three times using $ZnCl_2$ solution (1.5–1.7 $g \cdot mL^{-1}$) in order to eliminate the effect of the organic matter. Then, all of the $ZnCl_2$ extracts containing MPs were filtered three times using GF/B membranes (Whatman, UK; 1 μm pore size), and the membranes were placed in petri dishes and dried at 45 °C. The details of the extraction and analysis processes are described in Section S1 in Appendix A, and the significant testing results for the MPs from different locations are shown in Section S3 in the Appendix A.

2.4. Sediment grain size distribution analysis

The samples dissolved in H_2O_2 were further treated by adding 0.25 $mmol \cdot L^{-1}$ HCl to remove any calcium carbonate from the sediment. After settling, the upper solution was removed. Then, the samples were transferred to 50 mL centrifuge tubes, and 45 mL of ultrapure water was added. The samples in the centrifuge tubes were centrifuged at 5000 $r \cdot min^{-1}$ for 10 min; next, the supernatant was replaced with ultrapure water and the samples were re-centrifuged. The above operation was repeated several times until the pH of the solution was neutral. Once washed, each sample was transferred into a 50 mL beaker, and 5–10 mL of saturated $(NaPO_3)_6$ was added. The mixture was incubated for 24 h to completely disperse the sample. Finally, the size distribution of the sediment grains in the dispersion liquid was analyzed using a laser diffraction particle size analyzer (Malvern Mastersizer 3000, UK).

2.5. DNA extraction and polymerase chain reaction (PCR)

To extract the total genomic DNA, we used a FastDNA spin kit for soil (MP Biomedicals, USA) and followed the manufacturer's instructions. To evaluate the quality and purity of the DNA, we used both gel electrophoresis and a NanoDrop 2000 analyzer (Thermo Fisher Scientific, USA). Forward primer 340F (5′-CCCTAY-GGGGYGCASCAG-3′) and reverse primer 806rB (5′-GGAC-TACNVGGGTWTCTAAT-3′) were used to amplify the archaeal taxa [33]. For each sample, 30 cycles of PCRs were conducted in triplicate. The PCR products were checked via gel electrophoresis. Paired-end sequencing was conducted using an Illumina Miseq PE300 Sequencer system (USA).

2.6. Processing and analysis of sequencing data

The sequencing data were mainly processed and analyzed using VSEARCH v2.7.0 [34] and QIIME v1.9.0, with minor adjustments [35]. The adapter and low-quality (quality scores of 20) base pairs

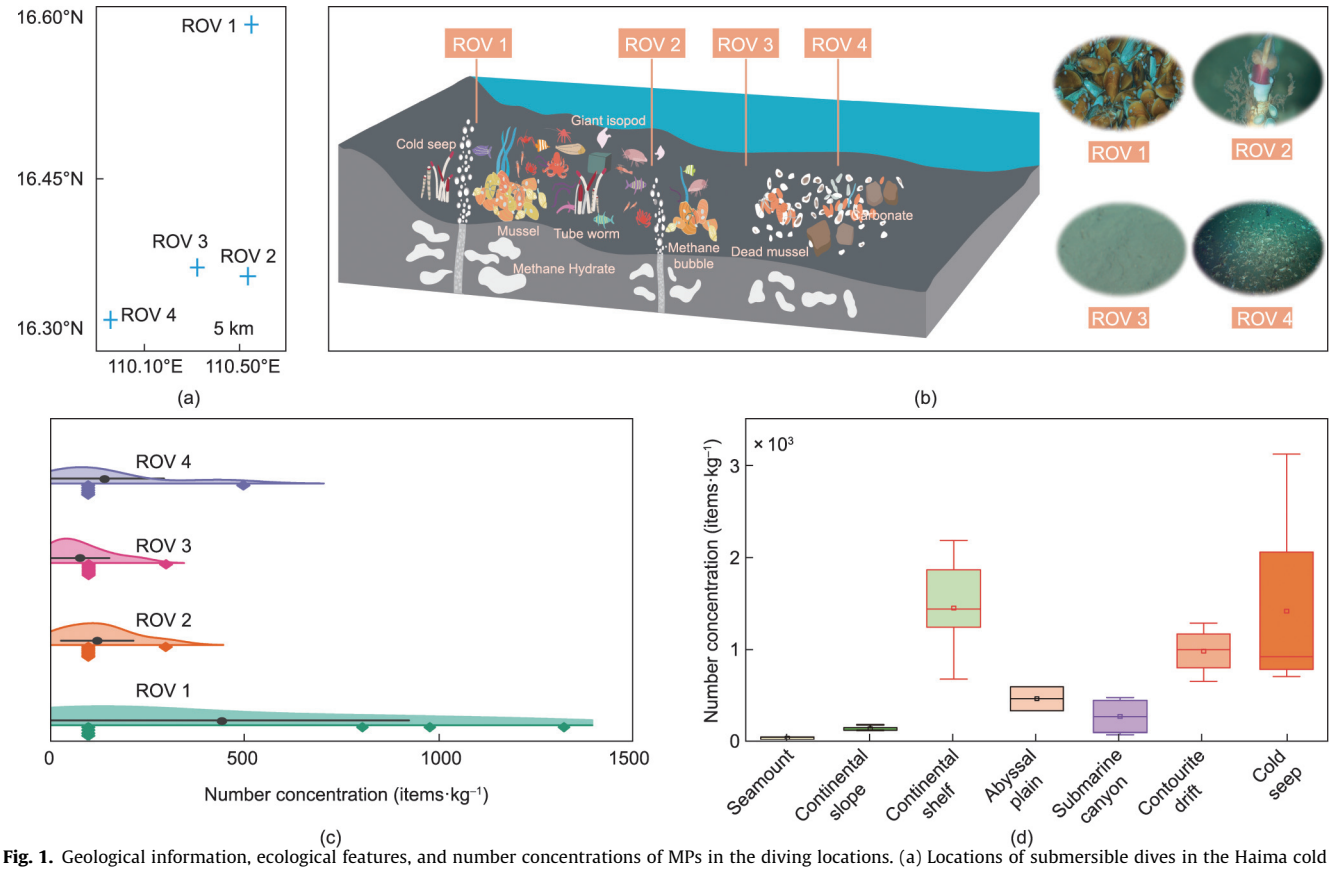

Fig. 1. Geological information, ecological features, and number concentrations of MPs in the diving locations. (a) Locations of submersible dives in the Haima cold seep in 2020. (b) Geological and biological features of the four areas were explored via a remotely operated vehicle (ROV). Detailed information about the basement rock in the sampling locations is shown in the oval panels. The location labeled as ROV 1 was characterized by strong active methane seepage, with continuous and enormous methane bubbles. ROV 2 was characterized by weak active methane seepage, with intermittent methane bubbles. Typical living indicator species, such as mussels, tubeworms, Alvin shrimp, and deep-sea crabs, were found at sites ROV 1 and ROV 2. There was no evidence of methane seeping or biological activity at site ROV 3. Site ROV 4 was characterized by large quantities of dead mussels and large blocks of carbonate but no indication of active methane seepage, indicating that historical methane-rich fluid seepage occurred in this area. (c) Number concentrations of MPs in different methane-seepage areas. Distribution of the number concentration was based on the size grading of the MPs into nine classes. (d) Comparison of number concentrations of MPs in cold seep sediments and other marine sediments [16,19,27–30].

(bp) were identified and trimmed from the ends of the raw paired-end reads using Trim Galore v0.4.5, followed by the removal of the short reads (< 100 bp). The paired-end reads were merged using VSEARCH, the primers were identified and cut out, quality filtering was performed to discard the low-quality reads (with > 1 total expected errors), and the sequences shorter than 300 bp were discarded. The operational taxonomic units (OTUs) were clustered at 97% identity using VSEARCH after removing the singletons (i.e., sequences that were present only once). Chimeras were detected and filtered using SILVA 132 [36]. The representative sequences of the OTUs were blasted in SILVA 132 using assign_taxonomy.py in QIIME v1.9.0.

3. Results

3.1. Enrichment and diversity of MPs in the Haima cold seep

The average number concentration of MPs in the Haima cold seep was found to be (1412.25 ± 570.15) items·kg^{-1} of sediment (Fig. 1(c)), which is the highest among that found in all types of ecological habitats in the deep sea, including the seamount, continental slope, abyssal plain, submarine canyon, and contourite drift environments (Fig. 1(d) [16,19,27–30]). The detailed information for the comparisons of MPs abundance in deep-sea environment are provided in Section S4 in the Appendix A. In this study, we analyzed the distribution of the MPs' surface areas in the surface of the deep-sea sediments using an LDIR system and found that the MPs' surface areas were significantly smaller than 1×10^3 μm^2 (Fig. 2(a)). The average surface area of the MPs in the Haima cold seep was (2273.38 ± 219.56) μm^2. The information of the scanning images, spectra, sizes, and areas of the detected MPs are provided in Figs. S3 and S4 in the Appendix A. The identified MPs were characterized as granular, fragment, fiber, foam, film, or linear (Fig. 2(b)), and the color of the MPs were mainly examined as blue, white, black, and red (Fig. 2(c)). A total of 16 types of MPs were found in the sediments of the Haima cold seep (Table S1 in Appendix A), among which polyurethane (PU), polyamide (PA), polyacetal (POM), and polyester (PET) were the most important components (Fig. 2(d)).

3.2. Influence of methane seepage on MP distribution

Interestingly, we found that the spatial distribution of the MPs in the Haima cold seep was correlated with the methane seepage. By counting the MPs in the sediments, we observed that the area with strong methane seepage (i.e., ROV 1) had a higher number concentration of MPs than the areas with weak seepage, no seepage, and historic seepage (i.e., ROV 2–ROV 4). The total number concentrations of sites ROV 1–ROV 4 were calculated as 3114, 981, 700, and 854 items·kg^{-1}, respectively. These findings encouraged us to continue to investigate the correlations between the size, shape, color, and material types of the MPs and the methane-seepage distribution.

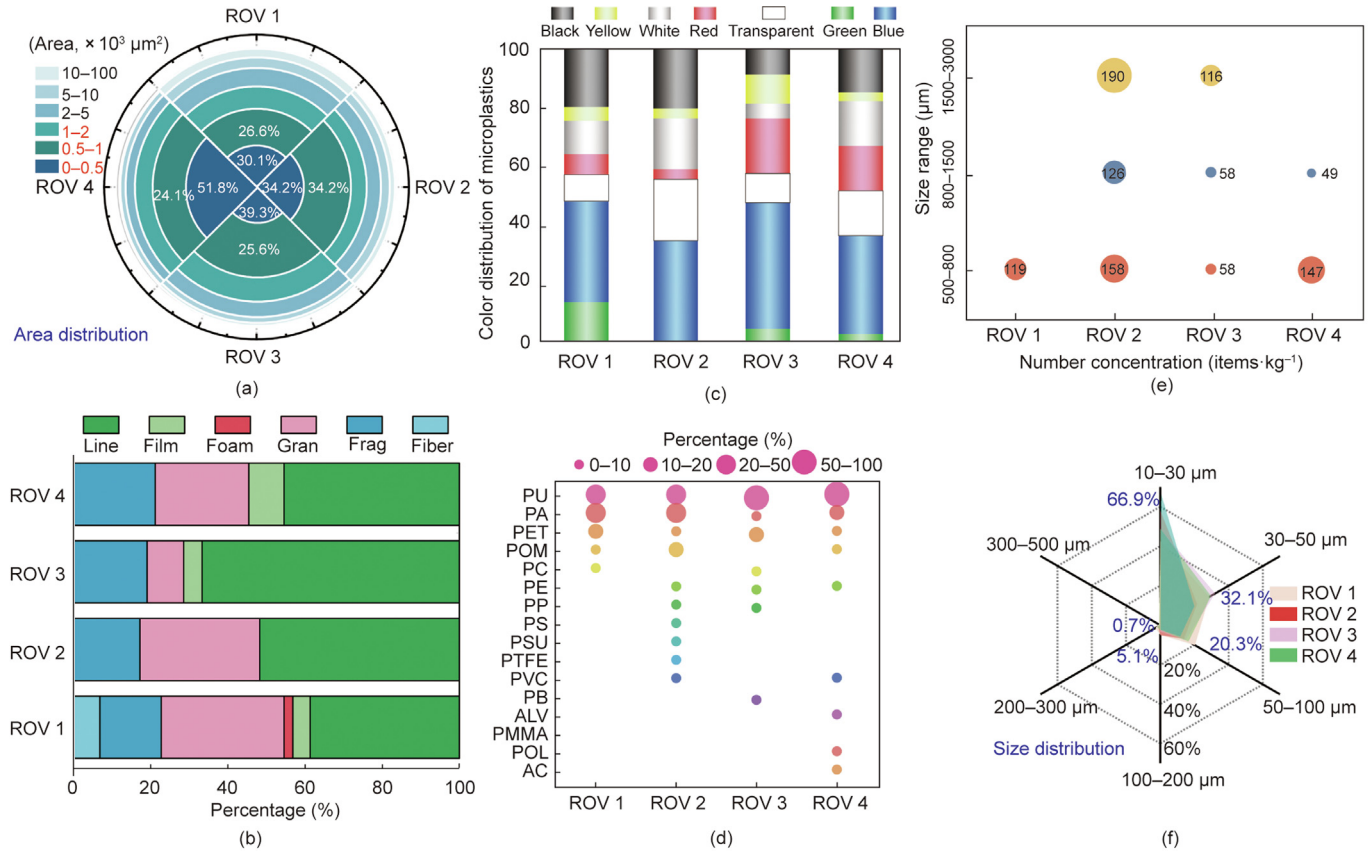

Fig. 2. Distributions of area, size, morphology, color, and category of MPs in sites ROV 1–ROV 4. (a) Area distribution of the identified MPs. (b) Proportions of MPs with different morphologies. Line: linear; gran: granular; frag: fragment. (c) Color distribution of detected MPs. (d) Sixteen categories of MPs distributed among the different locations in the Haima cold seep. PU: Polyurethane; PA: polyamide; PET: ethylene terephthalate; POM: polyacetal; PC: polycarbonate; PE: polyethylene; PP: polypropylene; PS: polystyrene; PSU: polysulfone; PTFE: polytetrafluoroethylene; PVC: poly vinyl chloride; PB: polybutadiene; ALV: alkyd varnish; PMMA: polymethyl methacrylate; POL: polyether; AC: acrylates. (e) Number abundance of MPs larger than 500 μm. (f) Number abundance of MPs smaller than 500 μm.

It should be noted that site ROV 1, which was characterized by strong plume leakage, had no large MPs (800–3000 μm) (Fig. 2(e)). Through a comparison of the size distributions of the MPs at the different seepage locations, we found that the size distributions of the MPs at the different locations were significantly different (Kruskal–Wallis test, $P = 6.82 \times 10^{-7}$; Fig. 2(f)). Linear MPs were dominant in the Haima cold seep, followed by granular MPs (images of the MPs are presented in Fig. S5 in Appendix A). It is very interesting that the abundance of the linear MPs tended to decrease as the methane seepage intensity increased, while the abundance of the granular MPs exhibited the opposite trend (Fig. 2(b)). The granular MPs accounted for the greatest proportion in the strong methane-seepage location (ROV 1), compared with the other locations. This location also had the highest diversity of MP morphologies, including linear, films, foams, granular, fragments, and fibers (Fig. 2(b)). The colors of the MPs found in the different methane-seepage environments were not significantly different (Kruskal–Wallis test, $P = 0.999$), and blue MPs were dominant in all of the locations in the Haima cold seep (Fig. 2(c)). However, we found that the material types of the MPs in the different methane-seepage environments were significantly different (Kruskal–Wallis test, $P = 4.48 \times 10^{-8}$; Fig. 2(d)). The diversity index of the category of MPs in the non-methane-seepage area (0.57) was the lowest, compared with those in the strong (1.31), weak (1.59), and historical (0.82) methane-seepage areas. The compositions of the large MPs (> 500 μm) at the four sampling locations were mainly polyethylene (PE) and polycarbonate (PC), according to FTIR analysis (Fig. S5).

3.3. Methane plumes cut into MPs and make their surfaces rougher

To understand how a strong methane-seepage environment makes MPs smaller, we further analyzed the mass concentrations of the MPs in the different regions of the Haima cold seep. The mass concentrations of the MPs in the ROV 1–ROV 4 sites were 77.76, 471.14, 409.03, and 297.37 mg·kg^{-1} sediment, respectively (Fig. 3(a)). It has been verified that smaller sediment grains can strongly accommodate fine MPs [37], and the sediment grain size of site ROV1 was the smallest (Fig. 3(b)), which contributed to the enrichment of smaller MPs in this location. Because the number concentration of MPs was the largest and the particles were the smallest in the strong methane-seepage area, we speculate that this may be related to the strong fluid fragmentation caused by the methane plume in the Haima cold seep.

As illustrated in Fig. 3(c), the lengths of the MPs were larger in the no-methane-seepage environment (ROV 3, blue triangle) than in the strong, weak, and historical methane-seepage environments, but their surface areas were not significantly larger. These findings prompted us to further explore the surface roughness of the MPs in the different methane-seepage environments. Based on scanning electron microscopy (SEM) analysis of the MPs' surfaces, we found that the surfaces of the MPs from the region without methane seepage (ROV 3) were very smooth, while the surfaces of the MPs from the regions with methane seepage were much rougher (Fig. 3(d)). Many burrs were present on the edges of the MPs from the strong methane-seepage (ROV 1) and weak methane-seepage (ROV 2) sites. In addition, the MPs from all of the methane-

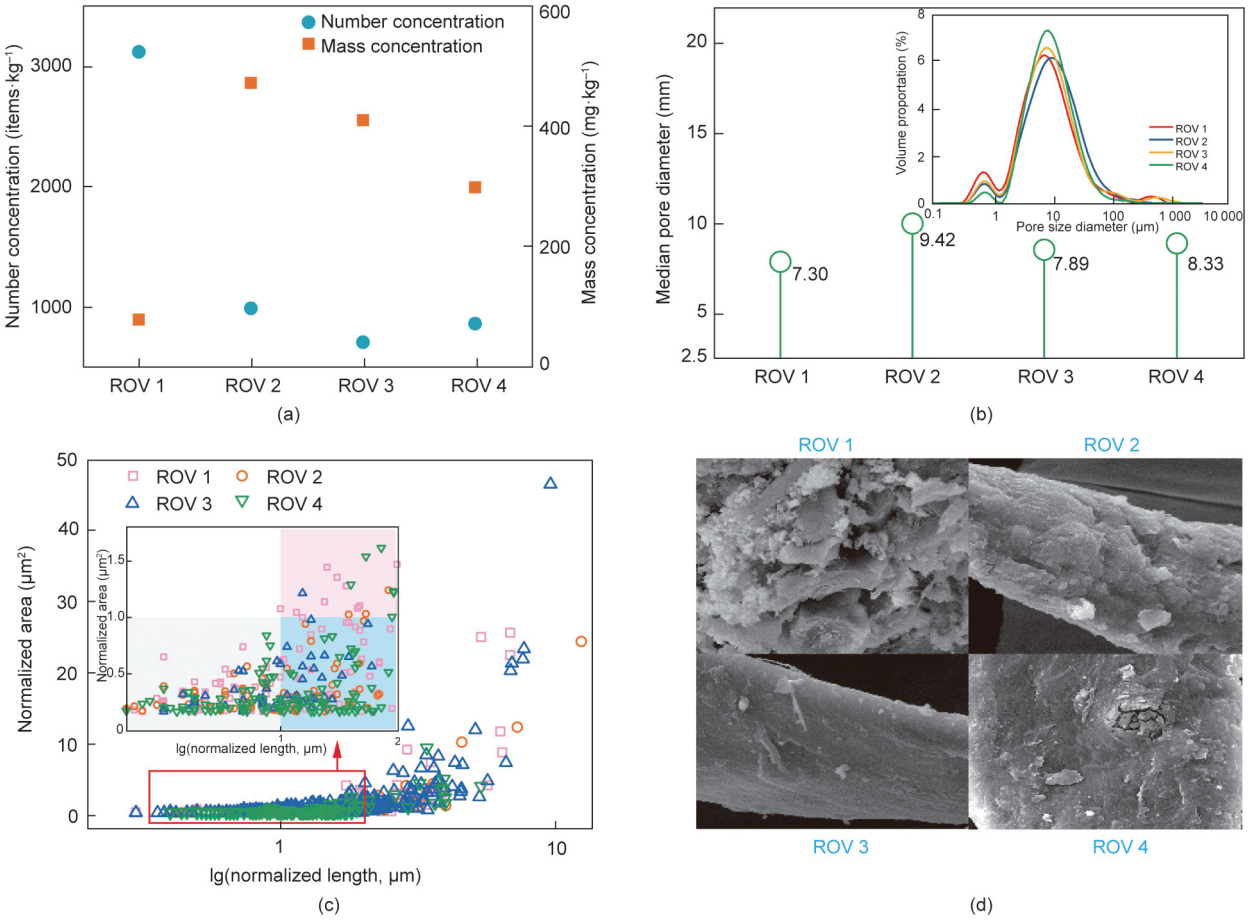

Fig. 3. Characterization of the fragmentation and surfaces of MPs. (a) Number and mass concentrations of MPs from the different locations. (b) Sediment grain size characteristics of the four sampling locations. (c) Relationship between normalized length and normalized area of small MPs (0–500 μm). (d) SEM images of the MPs from different locations.

seepage areas were observed to have layered exfoliation. In summary, the strong fluid fragmentation caused by the methane plume or methane seepage made the surfaces of the MPs even rougher.

3.4. MP sequestration can affect methane oxidization

The MPs of different shapes in the strong, weak, and historical methane-seepage areas generally had rougher external surfaces than those in the no-methane-seepage area. It is well-known that MPs can play a significant role in promoting heavy metal ion accumulation in marine environments [38], and the rough surfaces of the MPs may promote heavy metal aggregation. Therefore, we further explored the metal ion enrichment on the surfaces of the MPs from the different methane-seepage environments in the deep sea. Surface element analysis revealed that the indicator elements of marine water and pore water (e.g., Si, K, Ca, Sr, and Ba) were widely distributed on the surfaces of the MPs from the strong methane-seepage (ROV 1) and weak methane-seepage (ROV 2) sites (Fig. 4). It is noteworthy that, as a bulk element on the surface of the MPs, Fe accounted for 7% of the total quantity of all heavy metals on the MPs' surface at the strong methane-seepage site (ROV 1), and only 3.4% at the weak methane-seepage site (ROV 2) (Figs. 4(a) and (c)).

The accumulation of these heavy metals may serve important environmental and ecological functions in the cold seep ecosystem. A typical example is the Fe-driven AOM, which is ubiquitous in methane-seepage zones. In this metabolic process, iron oxides are important agents for the AOM, in which they act as electron acceptors during the methane oxidation process [34]. Methanotrophic bacteria participate in this metabolic process. They convert methane into organic matter that ultimately flows into the trophic cascade of the deep-sea ecosystem [39]. Based on an analysis of the microbial communities in the cold seep sediments, we found that methanomicrobia accounted for approximately 60% and 25% of all microorganism in the sediments from the strong and weak methane-seepage sites, respectively (Figs. 4(b) and (d)). At the class level, the observed methane oxidation via microorganisms was Fe-driven archaea [32]; for example, anaerbic methanotrophs (ANME)-1 and ANME-2 were widely distributed at sites ROV1 and ROV2, suggesting that the Fe enrichment on the MP surfaces may be beneficial to methane oxidation. Together, the specific enrichment of Fe and the microorganisms on the MPs with rougher external surfaces in the strong and weak methane-seepage environments may facilitate the dynamic AOM process, which may promote energy and material flow in the deep-sea ecosystem.

In summary, our results indicate that the deep-sea cold seep ecosystem is an MP enrichment funnel. The enrichment of MPs may have a positive effect on the energy and material circulation in the extreme deep-sea ecosystem to some extent, but its long-term impact on deep-sea organisms and ecosystems remains to be studied further in the future.

4. Discussion

4.1. The cold seep environment is an efficient MP sink

The particle sizes of the sediment samples were fine mud, with a median pore diameter of approximately 10 μm (Fig. 3(b)),

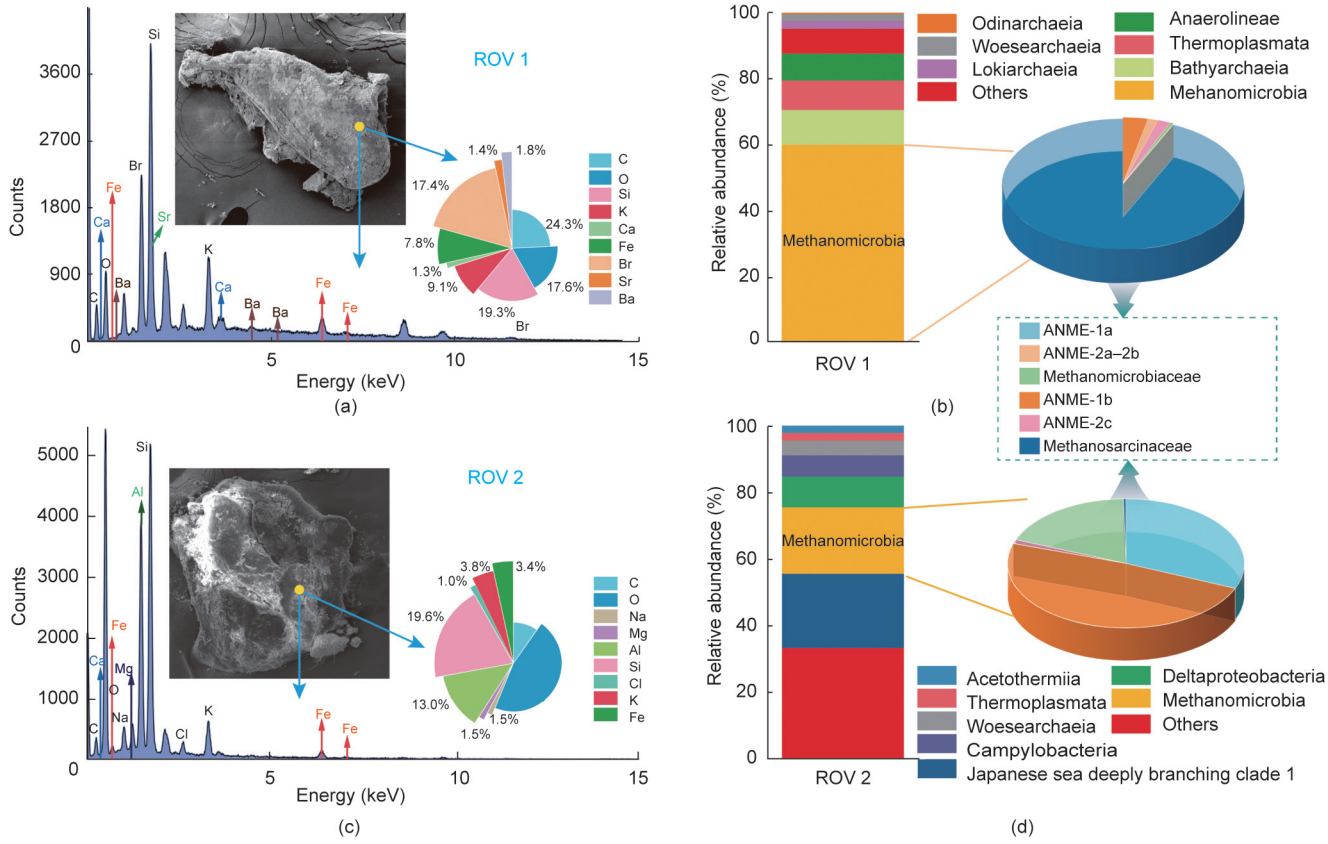

Fig. 4. Characteristics of the surface morphologies of the MPs, the elements adsorbed onto the MPs, and the microflora in the active methane-seepage areas. SEM-energy-dispersive X-ray spectroscopy (EDS) images of (a) ROV 1 and (c) ROV 2; Microflora of (b) ROV 1 and (d) ROV 2.

resulting in a sediment permeability of approximately 2.97 D [40] (1 D = 0.986923 × 10^{-12} m^2). The grain sizes of the sediments are shown in detail in Table S3 in Appendix A. Such a low permeability makes it difficult for fluids to flow through the sediment, and the silty-clay sediment is conducive to MP enrichment [41]. During the past decades, there has been no reconciliation of the sources, sinks, and stocks of MPs in the marine environment. The huge imbalance between the MPs floating on the sea surface and the annual amount of MPs discharged from rivers has led to a search for the missing MPs in marine water [42]. Marine and seafloor sediments have been considered to be huge sinks for MPs [43]. However, there is no global estimate of the MPs contained in marine sediments because of the limited number of samples and amount of data, especially in the extreme environment of the deep oceans. It is essential to clarify the percentage of MPs that can be deposited from the water column and the amount of MPs that can be captured and stored in these sediments on a global scale [13]. In this study, the occurrence of MPs in cold seep sediments was investigated for the first time. The substrates in the Haima cold seep are fine mud. The high percentage of clay in the cold seep sediments is beneficial to the accommodation of small MPs [11]. The geological environment and hydrodynamic conditions are important factors that control the distribution of MPs on the seafloor. We discovered that cold vents, from which methane spills out from its source in the deep sediments into the water column, govern the abundance and diversity of MPs in the sediments. For the assessment of an area, the abundance and diversity index have been demonstrated to be efficient indicators of the degree of MP pollution [44]. In our study, the strong methane-seepage area had the largest abundance of MPs and the highest diversity index. The diversity index values of the category of MPs in the active cold seep sites (ROV 1 and ROV 2) were more than twice that in the site without methane seepage (ROV3), suggesting that methane seepage increases the complex source of MPs in the sediments. As is shown in Fig. 5, recirculation flow and intrusion flow occurred at the rear of the methane plume in the seepage area [45]. Such unique fluid flow contributes to the transport and enrichment of small particles and MPs in the sediments.

A total of 16 types of MPs were detected (Fig. S6 in Appendix A), including PA, PB, PTFE, PVC, ALV, POM, PE, PC, PET, PP, PU, PS, PSU, POL, PMMA, and AC. Many more types than have been found in other discovered areas [46–48]. Of these, PU is known to be the fifth most abundant plastic in the world. PU paint has been widely applied on metal surfaces to prevent corrosion, and it is commonly used on the surface of ships and underwater cables. PA has the advantages of being firm and wear-proof. Engineering plastics made from PA can be used in the bearings and paddles of ships, as well as in ocean plates and underwater equipment [49]. POM is another type of high-performance engineering plastic. MPs can be generated from engineering plastics under the effects of hydrodynamic forces and ultraviolet radiation [50]. PET, the main component of plastic bottles, is common marine debris, and its degradation period can be longer than 15 years [51]. PC [52], PVC [38], PE [53], PP [54], and PS [55] have been extensively discovered in sediments in coastal regions and in sea water. However, these five primary types of MPs in coastal regions only accounted for a small proportion of the total MPs detected in the cold seep sediments analyzed in this study. In addition, seven uncommon types of MPs—namely, PSU, PTFE, PB, PMMA, AC, POL, and ALV—were detected in this study. PTFE is considered to be a durable high-quality plastic and is widely used for under cables, such as umbilical cables, because it is waterproof and resistant to low temperatures. PSU, PMMA, and POL can be utilized as electronic components or applied in marine engineering. AC, ACM, and ALV

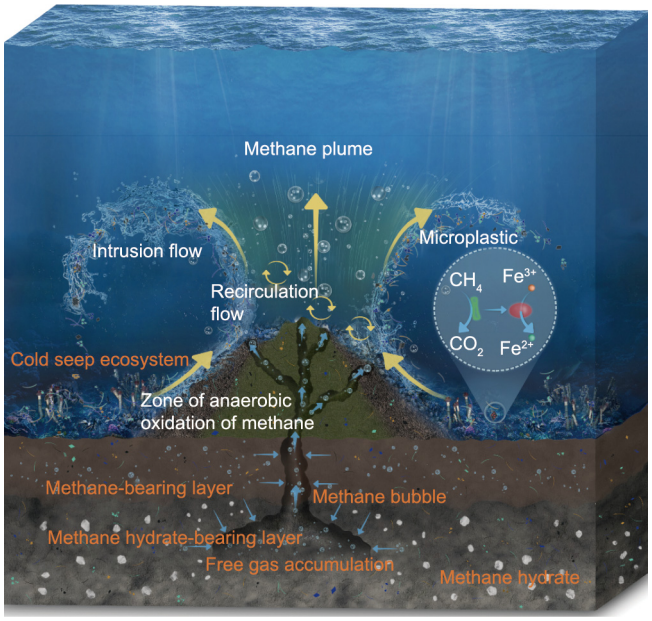

Fig. 5. Framework of the effects of MP enrichment in surface sediments by the upwelling methane-containing fluid flow, and the relationship between the Fe accumulated on MPs and the promotion of the anaerobic oxidation of methane during methane transportation. The colorful lines, blocks, and fragments represent the MPs. Blue arrows and transparent bubbles indicate the methane-seepage phenomenon of methane flow and methane bubbles, while yellow arrows denote the intrusion layer and recirculation flow of the methane-bearing fluid. Tube worms and mussels represent the cold seep ecosystem.

are important components of coatings and oil paints and are essential for marine monitoring, underwater equipment, and ship accessories. In particular, these offshore and underwater activities may generate MPs that can be buried in cold seep sediments—a process that has been overlooked until now.

The average number abundance of the MPs in the surface of the sediment was found to be higher in the cold seep than in other extreme ecosystems. However, cold seep communities possess a special metabolic pattern that relies on chemosynthesis and harvesting energy from methane [56]. Organisms living near cold seeps act as a benthic filter to absorb methane and prevent it from escaping into the upper part of the water column and the atmosphere, thereby playing an important role in the marine and global carbon cycles. Litter has been regarded as one of the major threats endangering cold seep ecosystems [57]; thus, long-term and large-scale monitoring of litter and MPs in the cold seep environment is extremely necessary. In the future, the relationship between the velocity of methane seepage and the behaviors of methane accumulation should be quantitatively monitored and assessed.

4.2. Interaction between methane seepage and MP sequestration

Previous studies have mainly determined the effects of hydrodynamic conditions on the distributions of MPs. The physical, chemical, and ecological feedbacks of MPs to the environment after their sequestration in the seafloor remain unclear. The results of this study indicate that methane seepage promotes the fragmentation of MPs. Small MPs can be ingested by and have great physiological toxicity to marine organisms, such as killer whales, turtles, and seabirds [26]. Therefore, in the future, the occurrence and ecotoxicology of MPs to cold seep organisms should receive serious attention.

The correlation between the length of MPs and the areas in which they are found could be an essential indicator of MPs that can be ingested by marine organisms or a tracer agent of the degree of MP fragmentation during transportation in marine environments. Based on the identification of such an indicator in detail, it is notable that, as shown in Fig. 3(c), the normalized length–area ratio of the MPs in the no-methane-seepage site (ROV3) is relatively smaller than the normalized length, indicating that MPs from the non-seepage site have relatively smooth surfaces. This can be attributed to the fact that the turbulent effect of the methane-bearing fluid flow can potentially enhance the aging process of the surface of the MPs. The SEM observations verified that the surfaces of the MPs from the methane-seepage locations were rougher, which is due to the fact that the MPs in these sediments were changed by the flushing effect of the ascending methane-bearing fluid. In addition, the microbial activities associated with methane generation and methane oxidation in the active cold seep area are quite high [58], and the activity of microbes attached to the surfaces of the MPs enhances the aging of the MPs [59]. The rough surfaces of the aged MPs are beneficial to the adsorbance of specific elements and microorganisms associated with methane metabolism. As can be seen from Fig. 4, archaea that perform methane anaerobic oxidation driven by ferric oxide and Fe were found on the surfaces of the MPs from the strong and weak methane-seepage sites, suggesting that the fragmentation and aging of MPs driven by methane fluid seepage are beneficial to the AOM. Methane oxidation provides basic energy and a carbon source for chemosynthesis in the cold seep environment, fueling the high level of metazoan biomass in the cold seeps [60]. In addition, methane oxidation acts as the main filter of methane associated with natural gas hydrate dissociation in the deep-sea environment [61]. Elucidating the mechanism and efficiency of iron ion-loading MPs in promoting the AOM necessitates field and laboratorial controlled and repeatable experiments, which will be carried out in the next work.

5. Conclusions

In summary, MPs' occurrence characteristics in the deep-sea cold seep sediment were investigated for the first time in this work. The combined testing method of LDIR and FTIR was used to test large-scale MP distribution (10–5000 μm), and the effectiveness of this method was verified by identifying a total of 16 types of MPs, which is far more than the number of types identified in previous work. Interestingly, the MP abundance in the surface of the sediment in the methane-seepage areas was greater than that in the non-seepage area. In addition, the strong seepage area had the greatest number abundance and the smallest mass abundance, as well as the largest diversity index. Furthermore, the surface of the MPs in the methane-seepage areas was rougher, indicating that methane-bearing fluid seepage is conducive to the accumulation, fragmentation, diversity, and aging of MPs in cold seep sediments. In turn, the sequestration of MPs in the seafloor can lead to the accumulation of iron ions on the MP surface, which can potentially promote the AOM, driven by metal ions. That is, MPs can serve as the intermediary of methane migration and transformation, accelerating the methane and carbon cycles in cold seeps. In the future, more attention should be paid to the interactions between methane migration, the carbon cycle, and the occurrence of MPs in the special and fragile ecosystems associated with cold seeps. More data, samples, and simulation models are essential.

Acknowledgments

This research was financially supported by the National Natural Science Foundation of China (42022046), the National Key Research and Development Program of China (2021YFF0502300), the Key Special Project for Introduced Talent Teams of the

Southern Marine Science and Engineering Guangdong Laboratory (Guangzhou) (GML2019ZD0403 and GML2019ZD0401), and Guangdong Natural Resources Foundation (GDNRC[2022]45).

Compliance with ethical guidelines

Jing-Chun Feng, Zhifeng Yang, Wenliang Zhou, Xingwei Feng, Fuwen Wei, Bo Li, Chuanxin Ma, Si Zhang, Linlin Xia, Yanpeng Cai, and Yi Wang declare that they have no conflicts of interest or financial conflicts to disclose.

Appendix A. Supplementary data

Supplementary data to this article can be found online at https://doi.org/10.1016/j.eng.2022.08.009.

References

[1] Jambeck JR, Geyer R, Wilcox C, Siegler TR, Perryman M, Andrady A, et al. Plastic waste inputs from land into the ocean. Science 2015;347(6223):768–71.
[2] Pabortsava K, Lampitt RS. High concentrations of plastic hidden beneath the surface of the Atlantic Ocean. Nat Commun 2020;11(1):4073.
[3] Cole M, Lindeque PK, Fileman E, Clark J, Lewis C, Halsband C, et al. Microplastics alter the properties and sinking rates of zooplankton faecal pellets. Environ Sci Technol 2016;50(6):3239–46.
[4] Teuten EL, Saquing JM, Knappe DRU, Barlaz MA, Jonsson S, Björn A, et al. Transport and release of chemicals from plastics to the environment and to wildlife. Philos Trans R Soc B 2009;364(1526):2027–45.
[5] Kooi M, Nes EHV, Scheffer M, Koelmans AA. Ups and downs in the ocean: effects of biofouling on vertical transport of microplastics. Environ Sci Technol 2017;51(14):7963–71.
[6] Van Cauwenberghe L, Vanreusel A, Mees J, Janssen CR. Microplastic pollution in deep-sea sediments. Environ Pollut 2013;182:495–9.
[7] Koelmans AA, Kooi M, Law KL, van Sebille E. All is not lost: deriving a top-down mass budget of plastic at sea. Environ Res Lett 2017;12(11):114028.
[8] Kukkola AT, Senior G, Maes T, Silburn B, Bakir A, Kröger S, et al. A large-scale study of microplastic abundance in sediment cores from the UK continental shelf and slope. Mar Pollut Bull 2022;178:113554.
[9] Jones ES, Ross SW, Robertson CM, Young CM. Distributions of microplastics and larger anthropogenic debris in Norfolk Canyon, Baltimore Canyon, and the adjacent continental slope (Western North Atlantic Margin, U.S.A.). Mar Pollut Bull 2022;174:113047.
[10] Peng G, Bellerby R, Zhang F, Sun X, Li D. The ocean's ultimate trashcan: hadal trenches as major depositories for plastic pollution. Water Res 2020;168:115121.
[11] Cunningham EM, Ehlers SM, Dick JTA, Sigwart JD, Linse K, Dick JJ, et al. High abundances of microplastic pollution in deep-sea sediments: evidence from Antarctica and the Southern Ocean. Environ Sci Technol 2020;54(21):13661–71.
[12] Gola D, Kumar Tyagi P, Arya A, Chauhan N, Agarwal M, Singh SK, et al. The impact of microplastics on marine environment: a review. Environ Nanotechnol Monit Manag 2021;16:100552.
[13] Stubbins A, Law KL, Muñoz SE, Bianchi TS, Zhu L. Plastics in the earth system. Science 2021;373(6550):51–5.
[14] Stabholz M, Durrieu de Madron X, Canals M, Khripounoff A, Taupier-Letage I, Testor P, et al. Impact of open-ocean convection on particle fluxes and sediment dynamics in the deep margin of the Gulf of Lions. Biogeosciences 2013;10(2):1097–116.
[15] Talley LD. Salinity patterns in the ocean-volume 1: the earth system: physical and chemical dimensions of global environmental change. In: MacCracken MC, Perry JS, editors. Encyclopedia of global change. Chichester, UK: John Wiley & Sons; 2002. p. 629–40.
[16] Kane IA, Clare MA, Miramontes E, Wogelius R, Rothwell JJ, Garreau P, et al. Seafloor microplastic hotspots controlled by deep-sea circulation. Science 2020;368(6495):1140–5.
[17] Canals M, Company JB, Martin D, Sanchez-Vidal A, Ramirez-Llodra E. Integrated study of Mediterranean deep canyons: novel results and future challenges preface. Prog Oceanogr 2013;118:1–27.
[18] Peng X, Chen M, Chen S, Dasgupta S, Xu H, Ta K, et al. Microplastics contaminate the deepest part of the world's ocean. Geochem Perspect Lett 2018:1–5.
[19] Woodall LC, Sanchez-Vidal A, Canals M, Paterson GLJ, Coppock R, Sleight V, et al. The deep sea is a major sink for microplastic debris. R Soc Open Sci 2014;1(4):140317.
[20] Boetius A, Wenzhofer F. Seafloor oxygen consumption fuelled by methane from cold seeps. Nat Geosci 2013;6(9):725–34.
[21] Leifer I. Characteristics and scaling of bubble plumes from marine hydrocarbon seepage in the Coal Oil Point seep field. J Geophys Res Oceans 2010;115(11):C11014.
[22] Wilson DS, Leifer I, Maillard E. Megaplume bubble process visualization by 3D multibeam sonar mapping. Mar Pet Geol 2015;68:753–65.
[23] Leifer I, Judd A. The UK22/4b blowout 20 years on: investigations of continuing methane emissions from sub-seabed to the atmosphere in a North Sea context. Mar Pet Geol 2015;68:706–17.
[24] Courtene-Jones W, Quinn B, Gary SF, Mogg AOM, Narayanaswamy BE. Microplastic pollution identified in deep-sea water and ingested by benthic invertebrates in the Rockall Trough, North Atlantic Ocean. Environ Pollut 2017;231(Pt 1):271–80.
[25] Botterell ZLR, Beaumont N, Cole M, Hopkins FE, Steinke M, Thompson RC, et al. Bioavailability of microplastics to marine zooplankton: effect of shape and infochemicals. Environ Sci Technol 2020;54(19):12024–33.
[26] MacLeod M, Arp HPH, Tekman MB, Jahnke A. The global threat from plastic pollution. Science 2021;373(6550):61–5.
[27] Vianello A, Boldrin A, Guerriero P, Moschino V, Rella R, Sturaro A, et al. Microplastic particles in sediments of Lagoon of Venice, Italy: first observations on occurrence, spatial patterns and identification. Estuar Coast Shelf Sci 2013;130:54–61.
[28] Bergmann M, Wirzberger V, Krumpen T, Lorenz C, Primpke S, Tekman MB, et al. High quantities of microplastic in Arctic deep-sea sediments from the HAUSGARTEN observatory. Environ Sci Technol 2017;51(19):11000–10.
[29] Sanchez-Vidal A, Thompson RC, Canals M, de Haan WP, Chin WC. The imprint of microfibres in southern European deep seas. PLoS ONE 2018;13(11):e0207033.
[30] Martin J, Lusher A, Thompson RC, Morley A. The deposition and accumulation of microplastics in marine sediments and bottom water from the Irish continental shelf. Sci Rep 2017;7:10772.
[31] Niu M, Fan X, Zhuang G, Liang Q, Wang F. Methane-metabolizing microbial communities in sediments of the Haima cold seep area, northwest slope of the South China Sea. FEMS Microbiol Ecol 2017;93(9):fix101.
[32] Beal EJ, House CH, Orphan VJ. Manganese- and iron-dependent marine methane oxidation. Science 2009;325(5937):184–7.
[33] Bahram M, Anslan S, Hildebrand F, Bork P, Tedersoo L. Newly designed 16S rRNA metabarcoding primers amplify diverse and novel archaeal taxa from the environment. Environ Microbiol Rep 2019;11(4):487–94.
[34] Rognes T, Flouri T, Nichols B, Quince C, Mahé F. VSEARCH: a versatile open source tool for metagenomics. PeerJ 2016;4:e2584.
[35] Kong J, Wang L, Lin C, Kuang F, Zhou X, Laws EA, et al. Contrasting community assembly mechanisms underlie similar biogeographic patterns of surface microbiota in the Tropical North Pacific Ocean. Microbiol Spectr 2022;10(1):e0079821.
[36] Yilmaz P, Parfrey LW, Yarza P, Gerken J, Pruesse E, Quast C, et al. The SILVA and "All-species Living Tree Project (LTP)" taxonomic frameworks. Nucleic Acids Res 2014;42(D1):D643–8.
[37] Sun X, Wang T, Chen B, Booth AM, Liu S, Wang R, et al. Factors influencing the occurrence and distribution of microplastics in coastal sediments: from source to sink. J Hazard Mater 2021;410:124982.
[38] Brennecke D, Duarte B, Paiva F, Cacador I, Canning-Clode J. Microplastics as vector for heavy metal contamination from the marine environment. Estuar Coast Shelf Sci 2016;178:189–95.
[39] Yang S, Lv Y, Liu X, Wang Y, Fan Q, Yang Z, et al. Genomic and enzymatic evidence of acetogenesis by anaerobic methanotrophic archaea. Nat Commun 2020;11(1):3941.
[40] Civan F. Chapter 5—porosity and permeability relationships of geological formations. In: Civan F, editor. Reservoir formation damage. Burlington: Gulf Professional Publishing; 2007. p. 125–53.
[41] Barrett J, Chase Z, Zhang J, Holl MMB, Willis K, Williams A, et al. Microplastic pollution in deep-sea sediments from the Great Australian Bight. Front Mar Sci 2020;7:576170.
[42] Weiss L, Ludwig W, Heussner S, Canals M, Ghiglione JF, Estournel C, et al. The missing ocean plastic sink: gone with the rivers. Science 2021;373(6550):107–11.
[43] Booth AM, Sørensen L. Microplastic fate and impacts in the environment. In: Rocha-Santos T, Costa M, Mouneyrac C, editors. Handbook of microplastics in the environment. Cham: Springer International Publishing; 2020. p. 1–24.
[44] Li C, Gan Y, Zhang C, He H, Fang J, Wang L, et al. "Microplastic communities" in different environments: differences, links, and role of diversity index in source analysis. Water Res 2021;188:116574.
[45] Li J, Roche B, Bull JM, White PR, Leighton TG, Provenzano G, et al. Broadband acoustic inversion for gas flux quantification—application to a methane plume at scanner pockmark, Central North Sea. J Geophys Res Oceans 2020;125(9):e2020JC016360.
[46] Wang Z, Su B, Xu X, Di D, Huang H, Mei K, et al. Preferential accumulation of small (< 300 μm) microplastics in the sediments of a coastal plain river network in eastern China. Water Res 2018;144:393–401.
[47] Van Cauwenberghe L, Devriese L, Galgani F, Robbens J, Janssen CR. Microplastics in sediments: a review of techniques, occurrence and effects. Mar Environ Res 2015;111:5–17.
[48] Ling SD, Sinclair M, Levi CJ, Reeves SE, Edgar GJ. Ubiquity of microplastics in coastal seafloor sediments. Mar Pollut Bull 2017;121(1–2):104–10.
[49] Reddy MS, Basha S, Adimurthy S, Ramachandraiah G. Description of the small plastics fragments in marine sediments along the Alang–Sosiya ship–breaking yard. India Estuar Coast Shelf Sci 2006;68(3–4):656–60.

[50] Jahan S, Strezov V, Weldekidan H, Kumar R, Kan T, Sarkodie SA, et al. Interrelationship of microplastic pollution in sediments and oysters in a seaport environment of the eastern coast of Australia. Sci Total Environ 2019;695:133924.
[51] Ioakeimidis C, Fotopoulou KN, Karapanagioti HK, Geraga M, Zeri C, Papathanassiou E, et al. The degradation potential of PET bottles in the marine environment: an ATR-FTIR based approach. Sci Rep 2016;6(1):23501.
[52] Wang G, Lu J, Li W, Ning J, Zhou L, Tong Y, et al. Seasonal variation and risk assessment of microplastics in surface water of the Manas River Basin, China. Ecotox Environ Safe 2021;208:111477.
[53] Zhao J, Ran W, Teng J, Liu Y, Liu H, Yin X, et al. Microplastic pollution in sediments from the Bohai Sea and the Yellow Sea. China Sci Total Environ 2018;640–1:637–45.
[54] Lei L, Wu S, Lu S, Liu M, Song Y, Fu Z, et al. Microplastic particles cause intestinal damage and other adverse effects in zebrafish *Danio rerio* and nematode *Caenorhabditis elegans*. Sci Total Environ 2018;619–20:1–8.
[55] Wang F, Shih KM, Li XY. The partition behavior of perfluorooctanesulfonate (PFOS) and perfluorooctanesulfonamide (FOSA) on microplastics. Chemosphere 2015;119:841–7.
[56] Vanreusel A, De Groote A, Gollner S, Bright M, Unsworth RKF. Ecology and biogeography of free-living nematodes associated with chemosynthetic environments in the deep sea: a review. PLoS ONE 2010;5(8):e12449.
[57] Angiolillo M, Gérigny O, Valente T, Fabri MC, Tambute E, Rouanet E, et al. Distribution of seafloor litter and its interaction with benthic organisms in deep waters of the Ligurian Sea (Northwestern Mediterranean). Sci Total Environ 2021;788:147745.
[58] Levin LA, Baco AR, Bowden DA, Colaco A, Cordes EE, Cunha MR, et al. Hydrothermal vents and methane seeps: rethinking the sphere of influence. Front Mar Sci 2016;3:72.
[59] Botterell ZLR, Beaumont N, Dorrington T, Steinke M, Thompson RC, Lindeque PK. Bioavailability and effects of microplastics on marine zooplankton: a review. Environ Pollut 2019;245:98–110.
[60] Bernardino AF, Levin LA, Thurber AR, Smith CR, Medina M. Comparative composition, diversity and trophic ecology of sediment macrofauna at vents, seeps and organic falls. PLoS ONE 2012;7(4):e33515.
[61] Ruppel CD, Kessler JD. The interaction of climate change and methane hydrates. Rev Geophys 2017;55(1):126–68.